ON A FINITE ELEMENT WITH EMBEDDED DISCONTINUITIES FOR NUMERICAL MODELING OF FRACTURE

J. Oliver, A.E. Huespe and S. Blanco
Technical University of Catalonia (UPC), Civil Engineering School, Barcelona, SPAIN

ABSTRACT

A finite element to capture strong discontinuities in fracture simulations is analyzed. The element belongs to the family of symmetric (variationally consistent) elementally enriched finite elements with embedded discontinuities and provides a kinematically optimal description of the strain field. The original element, by Lofti and Shing, is modified to remove the typical failure to pass the patch test. The variational format is set in a rate form so that the resulting formulation is made incremental along the time-like parameter, instead of in total form. As a result, elemental constant stress solutions can be fulfilled in elastic regimes and partially (time-step size dependent) satisfied in the fracture regimes. The resulting element is then expected to increase robustness in comparison with unsymmetrical elements of the same family and not to exhibit stress-locking. The element is implemented in the context of the Continuum Strong Discontinuity Approach (CSDA) using an isotropic continuum damage model and its performance is checked through the three-dimensional numerical simulation of the classical splitting test in fracture mechanics of concrete.

1 INTRODUCTION

Finite elements with embedded discontinuities have been extensively considered for purposes of modeling material fracture. They are based on the addition, to standard finite elements, of discontinuous displacement modes enriching their capability of capturing displacement jumps that characterize cracks or fractures (strong discontinuities). Two families can be clearly distinguished in the literature: 1) Finite elements with elemental enrichment i.e.: the support of the enriching modes is the element domain; the resulting additional degrees of freedom are attached to the elements crossed by the discontinuity path and they can be condensed at elemental level (Oliver, et al.[1]) and 2) Finite elements with nodal enrichment i.e.: the support of the enriching mode is the set of elements sharing the same node; the resulting additional degrees of freedom are attached to those nodes belonging to any element crossed by the discontinuity path and they belong to the general families of partition of unity methods or X-FEM methods (Moës, et al.[2]). Advantages and disadvantages can be found in both families. Nodal enrichment seems to lead to more stable formulations whereas elemental enrichment allows much smaller computational costs and easier implementations. This paper is devoted to a particular version of an elementally enriched finite element whose original development was presented in Lofti and Shing[3]. This element has been barely used due to a fundamental drawback: it fails to pas the path test for elementally constant stress fields: i.e.: in elastic regimes the incompatible modes activate, this affecting the original accuracy of the element. On the other hand, it exhibits very interesting features: 1) its elemental enrichment allows elemental condensation of the discontinuous modes, 2) due to its symmetric character, it is expected to exhibit a great robustness and c) since the kinematics allows rigid body motions at both sides of the element, it is expected not to lock. In the present work an incremental version of that element is presented. The essential difference with the original one is the incremental (in time) derivation and implementation of the formulation, which results into the exact fulfillment of the patch test in the elastic regimes and the approximate (time step size dependent) fulfillment in the failure regime.

1.1Unsymmetric kinematically and statically consistent formulation

Let us consider the rate from of the B.V.P of a solid, Ω with boundary $\partial\Omega$ and outward normal $\boldsymbol{\nu}$, experiencing a strong discontinuity of the displacement field $\mathbf{u}(\mathbf{x},t)$, in a failure surface S with normal $\mathbf{n}$ (see Figure 1), in the time interval of interest $[0,T]$:

$$\begin{aligned}
&\nabla\cdot\dot{\boldsymbol{\sigma}}+\rho_0\dot{\mathbf{b}}=\mathbf{0} && \forall(\mathbf{x},t)\in\Omega\times[0,T]\\
&\dot{\boldsymbol{\sigma}}\cdot\boldsymbol{\nu}=\dot{\mathbf{t}}^{*} && \forall(\mathbf{x},t)\in\Gamma_\sigma\times[0,T]\\
&\dot{\mathbf{u}}=\dot{\mathbf{u}}^{*} && \forall(\mathbf{x},t)\in\Gamma_u\times[0,T]\\
&\dot{\boldsymbol{\sigma}}^{+}_{\Omega/S}\cdot\mathbf{n}=\dot{\boldsymbol{\sigma}}^{-}_{\Omega/S}\cdot\mathbf{n} && \forall(\mathbf{x},t)\in S\times[0,T]\\
&\dot{\boldsymbol{\sigma}}^{+}_{\Omega/S}\cdot\mathbf{n}=\dot{\boldsymbol{\sigma}}_{S}\cdot\mathbf{n} && \forall(\mathbf{x},t)\in S\times[0,T]
\end{aligned} \tag{1}$$

Let us now consider a finite element discretization of typical size h on Ω. The finite dimensional space of the discretized displacements is described by:

$$\begin{aligned}
&\mathcal{V}^h\equiv\{\dot{\mathbf{u}}(\mathbf{x},t)\ ;\ \dot{\mathbf{u}}=\sum_{i=1}^{n_i}N_i(\mathbf{x})\dot{\mathbf{u}}_i(t)+\mathcal{M}_S^{(e)}(\mathbf{x})\dot{\boldsymbol{\beta}}_e(t)\}\\
&\mathcal{M}_S^{(e)}(\mathbf{x})=\mathcal{H}_S^{(e)}(\mathbf{x})-\varphi^{(e)}(\mathbf{x})\ ;\ \varphi^{(e)}(\mathbf{x})=\sum_{i=1}^{n_e^+}N_{i^+}(\mathbf{x})\\
&\nabla\mathcal{M}_S^{(e)}(\mathbf{x})=\delta_S^{e)}(\mathbf{x})\mathbf{n}^{(e)}-\nabla\varphi^{(e)}(\mathbf{x})\approx\frac{\mu_S^{(e)}(\mathbf{x})}{k}\mathbf{n}^{(e)}-\nabla\varphi^{(e)}(\mathbf{x})\\
&\mu_S^{(e)}(\mathbf{x})=\begin{cases}1 & \forall\mathbf{x}\in S\\ 0 & otherwise\end{cases}\\
&\dot{\boldsymbol{\varepsilon}}=(\nabla\otimes\dot{\mathbf{u}})^{sym}=\underbrace{\dot{\underline{\underline{\boldsymbol{\varepsilon}}}}}_{regular}+\underbrace{\frac{\mu_S^{(e)}(\mathbf{x})}{k}\left(\mathbf{n}^{(e)}\otimes\dot{\boldsymbol{\beta}}_e\right)^{sym}}_{singular\ (unbounded)}
\end{aligned} \tag{2}$$

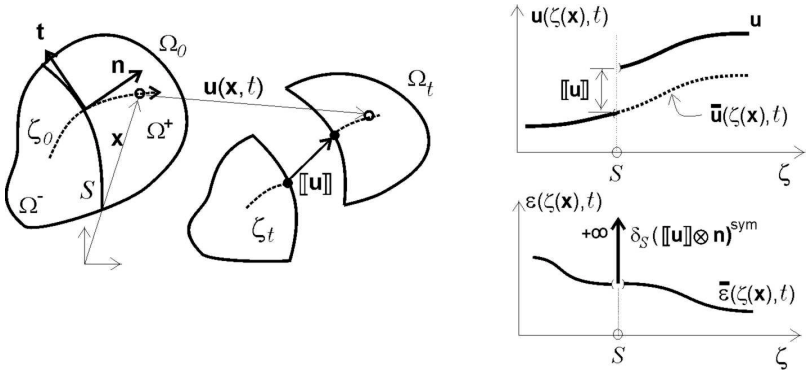

Figure 1: Strong discontinuity kinematics.

where $\mathcal{M}_S^{(e)}$ is the so called unit ramp function Oliver, et al.[1], $\mathbf{u}_i(t)$ stands for displacement at the regular nodes, i, and $\boldsymbol{\beta}_e$ are the elemental additional degrees of freedom representing the displacement jumps at those elements, e, crossed by S. For computational purposes the Dirac's

delta function $\delta_S^{e)}(\mathbf{x})$, emerging in equation (2) from the differentiation of the step function $\mathcal{H}_S^{(e)}$, is regularized in terms of a collocation function $\mu_S^{(e)}(\mathbf{x})$ on S and a regularization parameter, k, as small as permitted by the computer precision. The strain field $\dot{\boldsymbol{\varepsilon}}$ exhibits, as usual in the Continuum Strong Discontinuity approach, a regular (bounded) part and s singular (unbounded) component. Considering, the following space for the test functions (virtual displacements):

$$\mathcal{V}_0^h \equiv \{\boldsymbol{\eta}^h(\mathbf{x},t) \;;\; \boldsymbol{\eta}^h = \sum_{i=1}^{n_e} N_i(\mathbf{x})\boldsymbol{\eta}_i(t) + \boldsymbol{\mathcal{M}}_S^{(e)}(\mathbf{x})\tilde{\boldsymbol{\eta}}_e(t) \;\;;\;\; \boldsymbol{\eta}_i|_{\Gamma_u} = 0\} \tag{3}$$

the variational principle (virtual work principle):

$$\delta\Pi(\dot{\mathbf{u}};\boldsymbol{\eta}^h) \equiv \int_\Omega \nabla^S \boldsymbol{\eta}^h : \dot{\boldsymbol{\sigma}} d\Omega - \left[\int_\Omega \boldsymbol{\eta}^h \cdot \rho_0 \dot{\mathbf{b}} dV + \int_{\Gamma_\sigma} \boldsymbol{\eta}^h \cdot \dot{\mathbf{t}}^* d\Gamma\right] = \mathbf{0} \;\;;\;\; \forall \boldsymbol{\eta}^h \in \mathcal{V}_0^h \tag{4}$$

defines a symmetric (Galerkin type) formulation which qualifies the element as *symmetric kinematically consistent* (Oliver, et al.[1], Jirasek[4]).

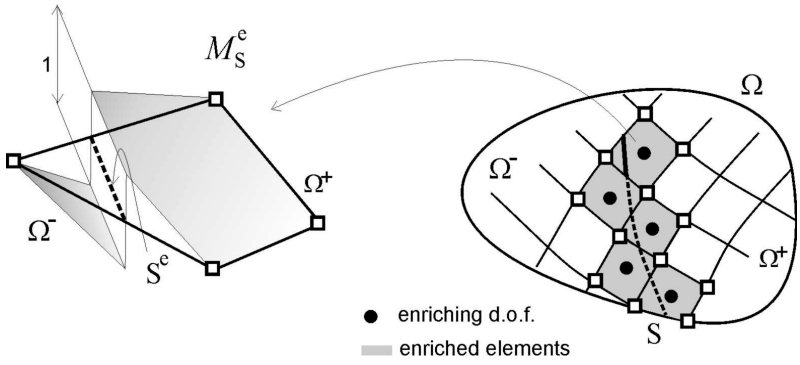

Figure 2: Finite element with elemental enrichment

1.2 Incremental approach.

In the context of a quasi-static problem ruled by the time-like parameter t during a discrete number of time steps, n_{int}, of typical length Δt:

$$t \in [0,T] = \bigcup_0^{n_{\text{int}}} [t_n, t_{n+1}] \;\;;\;\; t_{n+1} - t_n = \Delta t \tag{5}$$

the variational principle (4) can be integrated leading to the following non linear problem in interval $[t_n, t_{n+1}]$:

$$\int_\Omega \nabla^S \boldsymbol{\eta}^h : (\boldsymbol{\sigma}_{n+1} - \boldsymbol{\sigma}_n) d\Omega - \left[\int_\Omega \boldsymbol{\eta}^h \cdot \rho_0 (\mathbf{b}_{n+1} - \mathbf{b}_n) d\Omega + \int_{\Gamma_\sigma} \boldsymbol{\eta}^h \cdot (\mathbf{t}^*_{n+1} - \mathbf{t}^*_n) d\Gamma\right] = 0 \quad \forall \boldsymbol{\eta}^h \in \mathcal{V}_0^h \tag{6}$$

which can be rearranged giving rise to the following set of non linear equations:

$$\underbrace{\begin{Bmatrix} \int_{\Omega} \nabla^{S} N_i \cdot \boldsymbol{\sigma}_{n+1} d\Omega \\ \\ \int_{\Omega^{(e)}} \nabla^{S} \boldsymbol{\mathcal{M}}_{S}^{(e)} \cdot (\boldsymbol{\sigma}_{n+1} - \boldsymbol{\sigma}_{n})\, d\Omega \end{Bmatrix}}_{\mathbf{F}_{\text{int}}(\mathbf{u}_i, \boldsymbol{\beta}_e)_{n+1}} = \underbrace{\begin{Bmatrix} \left[\int_{\Omega} N_i\, \rho_0 \mathbf{b}_{n+1} dV + \int_{\Gamma_\sigma} N_i\, \mathbf{t}^{*}_{n+1}\, d\Gamma \right] \\ \\ \mathbf{0} \end{Bmatrix}}_{\mathbf{F}_{ext\, n+1}} \quad \begin{matrix} \forall i \in \{1...., n_{node}\} \\ \\ \forall e \in \{1...., n_{elem}\} \end{matrix} \tag{7}$$

The specific (incremental) format of the second set of equations in (7) allows overcoming a crucial drawback of the symmetric kinematically optimal finite element with a embedded discontinuity: *the failure in passing the patch test for elementary piecewise constant stress fields* (as in elastic solutions). In fact, from the expression of $\boldsymbol{\mathcal{M}}_{S}^{(e)}(\mathbf{x})$ in equation (2) it can be readily shown that:

$$\int_{\Omega^{(e)}} \nabla \boldsymbol{\mathcal{M}}_{S}^{(e)} \cdot (\boldsymbol{\sigma}_{n+1} - \boldsymbol{\sigma}_{n}) d\Omega \neq \mathbf{0} \quad for \quad \begin{cases} \boldsymbol{\sigma}_{n+1}(\mathbf{x}) = \text{constant} \quad \text{in} \quad \Omega^{(e)} \\ \boldsymbol{\sigma}_{n}(\mathbf{x}) = \text{constant} \quad \text{in} \quad \Omega^{(e)} \end{cases} \tag{8}$$

unlike what is required for that elastic patch test criterion. As a result, the enriching incompatible modes for a given element will activate even before the material failure of that element; this substantially affects the accuracy of the element at stages prior to the material failure. However, the incremental character of equation (7) reveals that:

$$\int_{\Omega^{(e)}} \nabla \boldsymbol{\mathcal{M}}_{S}^{(e)} \cdot (\boldsymbol{\sigma}_{n+1} - \boldsymbol{\sigma}_{n}) d\Omega = \mathcal{O}(\Delta t) \rightarrow \mathbf{0} \tag{9}$$

and, therefore, that the patch test criterion tends to be fulfilled with decreasing time steps ($\Delta t \rightarrow 0$). Therefore *refinement in the time-like domain leads to the fulfillment of the patch test in the space domain*. In a subsequent manipulation, equations (7) can be modified as:

$$\underbrace{\begin{Bmatrix} \int_{\Omega} \nabla^{S} N_i \cdot \boldsymbol{\sigma}_{n+1} d\Omega \\ \\ \int_{\Omega^{(e)}} \nabla^{S} \boldsymbol{\mathcal{M}}_{S}^{(e)} \cdot (\boldsymbol{\sigma}_{n+1} - \boldsymbol{\sigma}_{n}) - d\Omega \end{Bmatrix}}_{\mathbf{F}_{\text{int}}(\mathbf{u}_i, \boldsymbol{\beta}_e)_{n+1}} = \underbrace{\begin{Bmatrix} \left[\int_{\Omega} N_i\, \rho_0 \mathbf{b}_{n+1} dV + \int_{\Gamma_\sigma} N_i\, \mathbf{t}^{*}_{n+1}\, d\Gamma \right] \\ \\ \mathbf{0} \end{Bmatrix}}_{\mathbf{F}_{ext\, n+1}} \quad \begin{matrix} \forall i \in \{1...., n_{node}\} \\ \{\forall e \in \{1...., n_{elem}\} \\ \{\forall t_n \geq t_B^{(e)} \end{matrix} \tag{10}$$

where $t_B^{(e)}$ stands for the time of the onset of the material failure at element e. This precludes the activation of the incompatible discontinuous modes during the elastic regime and returns to the element its original accuracy at stages prior to the onset of material failure.

The algorithmic tangent stiffness of the iterative Newton-Raphson scheme for the nonlinear problem (10) at time step $n+1$ then reads:

$$\underbrace{\begin{bmatrix} \mathbf{K}_{uu} & \mathbf{K}_{u\beta} \\ \mathbf{K}^{T}{}_{u\beta} & \mathbf{K}_{\beta\beta} \end{bmatrix}^{(i)}_{n+1}}_{\mathbf{K}^{(i)}_{n+1}} \begin{bmatrix} \delta\mathbf{u}^{(i)} \\ \delta\boldsymbol{\beta}^{(i)} \end{bmatrix} = [\mathbf{F}_{ext} - \mathbf{F}_{\text{int}}]^{(i)}_{n+1} \quad ; \quad \begin{cases} \delta\mathbf{u}^{(i)} = \{\delta\mathbf{u}^{(i)}_{1}, ...\delta\mathbf{u}^{(i)}_{n_{node}}\}^{T} \\ \delta\boldsymbol{\beta}^{(i)} = \{\delta\boldsymbol{\beta}^{(i)}_{1}, ...\delta\boldsymbol{\beta}^{(i)}_{n_{elem}}\}^{T} \end{cases}$$

$$\left.\begin{aligned} \mathbf{K}_{uu} &= \boldsymbol{\mathcal{A}}(\mathbf{K}^{(e)}_{uu}) \quad ; \quad \left[\mathbf{K}^{(e)}_{uu}\right]_{ij} = \int_{\Omega^{(i)}} \nabla N_i \cdot \mathbf{C}^{\text{alg}} \cdot \nabla N_j d\Omega \\ \mathbf{K}_{\beta\beta} &= \boldsymbol{\mathcal{A}}(\mathbf{K}^{(e)}_{\beta\beta}) \quad ; \quad \mathbf{K}^{(e)}_{\beta\beta} = \int_{\Omega^{(e)}} \nabla \boldsymbol{\mathcal{M}}_{S}^{(e)} \cdot \mathbf{C}^{\text{alg}} \cdot \nabla \boldsymbol{\mathcal{M}}_{S}^{(e)} d\Omega \\ \mathbf{K}_{u\beta} &= \boldsymbol{\mathcal{A}}(\mathbf{K}^{(e)}_{u\beta}) \quad ; \quad \mathbf{K}^{(e)}_{\beta\beta} = \int_{\Omega^{(e)}} \nabla N_i \cdot \mathbf{C}^{\text{alg}} \cdot \nabla \boldsymbol{\mathcal{M}}_{S}^{(e)} d\Omega \end{aligned}\right\} \quad i, j \in \{1,..., n^{(e)}_{node}\} \tag{11}$$

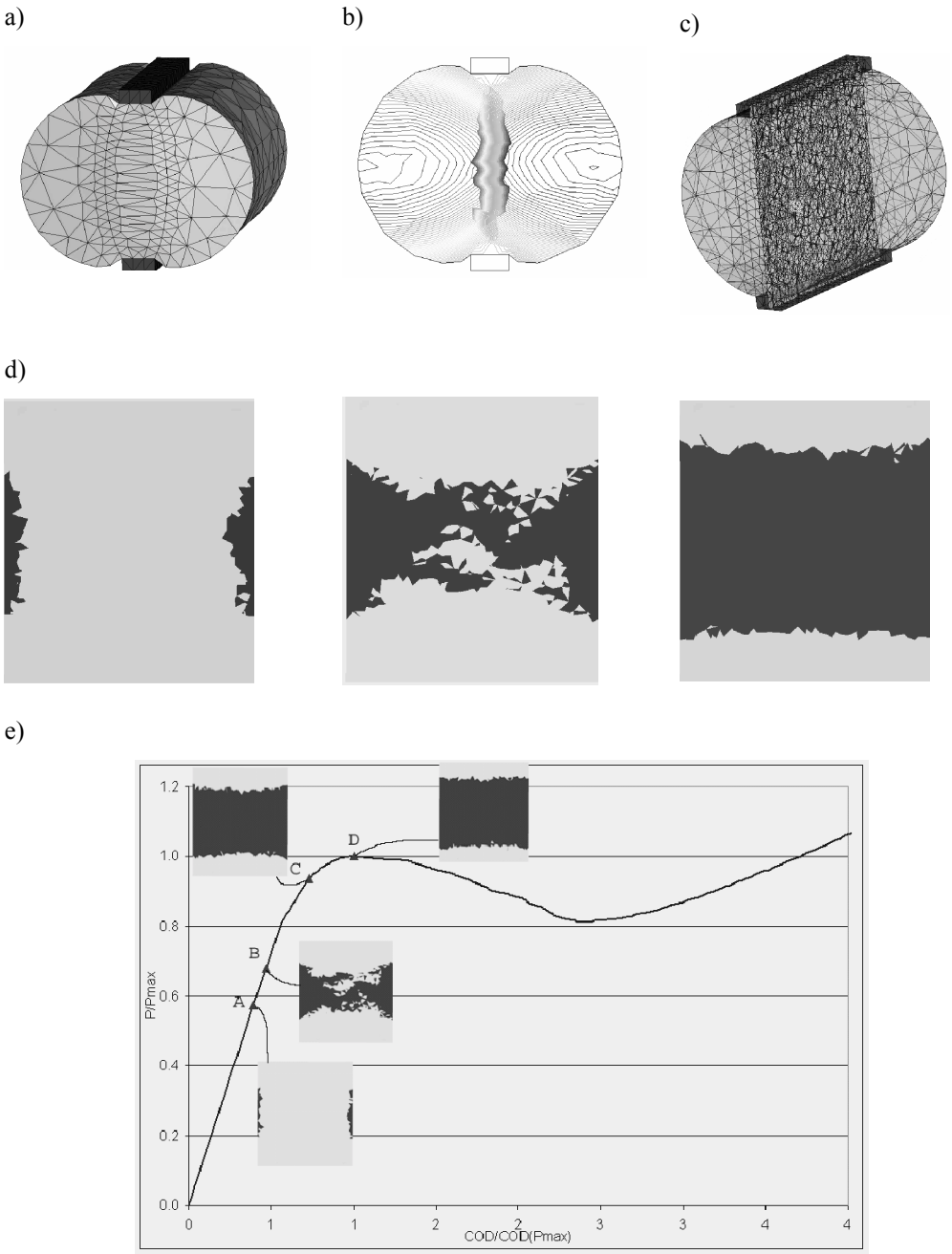

Figure 3: Three-dimensional simulation of the splitting test: a) finite element discretization (tetrahedra) and deformation pattern, b) displacement contours displaying localization at the central row of elements, c) captured cracking surface, d) evolution along time of the cracking (in dark) on the central surface and e) vertical force vs. vertical top displacement curve.

where $\mathcal{A}(\cdot)$ stands for the assembling operator. and $\delta(\cdot)^{(i)}$ stands for the iterative variation of the degree of freedom $(\cdot)$ at iteration i. In equation (11) the algorithmic tangent constitutive operator, $\mathbf{C}^{\text{alg}}$, emerges from integration of a chosen (material dependent) dissipative continuum constitutive model equipped with strain softening:

$$\begin{aligned} &\boldsymbol{\sigma}_{n+1} = \sum(\boldsymbol{\varepsilon}_{n+1}, \mathcal{H}) \;\; ; \;\; \frac{\sum(\boldsymbol{\varepsilon}_{n+1})}{\partial \boldsymbol{\varepsilon}_{n+1}} = \mathbf{C}^{\text{alg}}_{n+1} \\ &\mathcal{H} = h\overline{\mathcal{H}} \;\; ; \;\; \overline{\mathcal{H}} = \frac{1}{2}\frac{\sigma_y^2}{G_f} \end{aligned} \tag{12}$$

where $\mathcal{H}$ stands for the softening modulus of the model, which is regularized (using the same regularization parameter, k, than in the kinematics in equation (2)) in terms of the intrinsic softening modulus, $\overline{\mathcal{H}}$. This parameter captures the actual fracturing properties of the material in terms of the uniaxial strength σ_y and the fracture energy G_f.

From equations (11) it can be readily observed that, due to the symmetric character of the chosen formulation, *the positive definite character of the stiffness matrix* $\mathbf{K}^{(i)}_{n+1}$ *of the linearized problem can be guaranteed whenever the tangent constitutive operator* $\mathbf{C}^{\text{alg}}$ *is positive definite*. This fact confers to this element additional stability properties that can be conveniently exploited for numerical simulations.

2 REPRESENTATIVE SIMULATION

2.1 Three dimensional simulation of the cylindrical splitting test.

The classical splitting test in fracture mechanics of concrete is modeled using the finite element described above. The mechanical behavior of concrete is captured using an isotropic continuum damage model, which is made sensitive only to tensile damage (Oliver, et al.[5]). Although standard material properties of concrete have been taken, the simulation is essentially qualitative and attempts to show that 3D simulations can be performed in small computers (PC's) in reduced computational times (less than one hour) as well as displaying some typical information that can be obtained in the analysis (see Figure 3).

REFERENCES

[1] J. Oliver, A.E. Huespe, and E. Samaniego. A study on finite elements for capturing strong discontinuities. *Int.J.Num.Meth.Engng.* **56**, 2135-2161, 2003.

[2] N. Moës, N. Sukumar, B. Moran, and T. Belytschko. An extended finite element method (X-FEM) for two and three-dimensional crack modelling. presented at ECCOMAS 2000, Barcelona, Spain, 2000.

[3] H. R. Lofti and P. B. Shing. Embedded Representation of Fracture in Concrete with Mixed Finite-Elements. *International Journal for Numerical Methods in Engineering*. **38**, 1307-1325, 1995.

[4] M. Jirasek. Comparative study on finite elements with embedded discontinuities. *Computer Methods in Applied Mechanics and Engineering*. **188**, 307-330, 2000.

[5] J. Oliver, A. Huespe, M.D.G. Pulido, and E. Chaves. From continuum mechanics to fracture mechanics: the strong discontinuity approach. *Engineering Fracture Mechanics*. **69**, 113-136, 2002.